LAWRENCE
LIVERMORE
NATIONAL
LABORATORY

Laboratory astrophysical collisionless shock experiments on Omega and NIF

H. S. Park, J. S. Ross, C. M. Huntington, F. Fiuza, D. Ryutov, D. Casey, R. P. Drake, G. Fiksel, D. Froula, G. Gregori, N. Kugland, C. Kuranz, M. Levy, C. K. Li, J. Meinecke, T. Morita, R. Petrasso, C. Plechaty, B. Remington, Y. Sakawa, A. Spitkovsky, H. Takabe, A. B. Zylstra

November 11, 2013

Disclaimer

This document was prepared as an account of work sponsored by an agency of the United States government. Neither the United States government nor Lawrence Livermore National Security, LLC, nor any of their employees makes any warranty, expressed or implied, or assumes any legal liability or responsibility for the accuracy, completeness, or usefulness of any information, apparatus, product, or process disclosed, or represents that its use would not infringe privately owned rights. Reference herein to any specific commercial product, process, or service by trade name, trademark, manufacturer, or otherwise does not necessarily constitute or imply its endorsement, recommendation, or favoring by the United States government or Lawrence Livermore National Security, LLC. The views and opinions of authors expressed herein do not necessarily state or reflect those of the United States government or Lawrence Livermore National Security, LLC, and shall not be used for advertising or product endorsement purposes.

Laboratory astrophysical collisionless shock experiments on Omega and NIF

Hye-Sook Park[1,*], J. S. Ross[1], C. M. Huntington[1], F. Fiuza[1], D. Ryutov[1], D. Casey[1], R. P. Drake[2], G. Fiksel[3], D. Froula[3], G. Gregori[4] , N. Kugland[5], C. Kuranz[2], M. Levy[1], C. K. Li[6], J. Meinecke[4], T. Morita[7], R. Petrasso[6], C. Plechaty[1], B. Remington[1], Y. Sakawa[7], A Spitkovsky[8], H. Takabe[7], A. B. Zylstra[6]

[1] Lawrence Livermore National Lab, 7000 East Ave, Livermore CA, USA
[2] Dept. of Atmospheric, Oceanic, and Space Sciences, University of Michigan, Ann Arbor, MI, USA
[3] Laboratory for Laser Energetics, Rochester, NY, USA
[4] University of Oxford, Oxford, UK
[5] Lam Research Corporation, 4400 Cushing Parkway, Fremont, CA, USA
[6] Massachusetts Institute of Technology, Cambridge, MA, USA
[7] Institute of Laser Engineering, Osaka University, Osaka, Japan
[8] Dept. of Astrophysical Sciences, Princeton University, Princeton, NJ, USA

*E-mail: park1@llnl.gov

Abstract. We are performing scaled astrophysics experiments on Omega and on NIF. Laser driven counter-streaming interpenetrating supersonic plasma flows can be studied to understand astrophysical electromagnetic plasma phenomena in a laboratory setting. In our Omega experiments, the counter-streaming flow plasma state is measured using Thomson scattering diagnostics, proving the plasma flows are indeed super-sonic and in the collisionless regime. We observe a surprising additional electron and ion heating from ion drag force in the double flow experiments that are attributed to the ion drag force and electrostatic instabilities. A proton probe is used to image the magnetic fields. We observe unexpected large, stable and reproducible electromagnetic field structures that arise in the counter-streaming flows [1]. The Biermann battery field generated near the target plane advects along the flows and recompresses near the midplane explains the cause of such self-organizing field structures [2]. A D^3He implosion proton probe image showed very clear filamentary structures. Three-dimensional Particle-In-Cell simulations and simulated proton radiography images indicate that these filamentary structures are generated by Weibel instabilities and that the magnetization level (ratio of magnetic energy over kinetic energy in the system) is ~0.01 [3]. These findings have very high astrophysical relevance and significant implications. We expect to observe true collisionless shock formation when we use >100 kJ laser energy on NIF.

1. Introduction

Astrophysical collionless shocks have been of keen interests to the astrophysical community as a mechanism for self-generating magnetic fields and cosmic ray acceleration. Collisionless shock is the condition where the Coulomb mean free path is much larger than the system, yet a shock is formed via plasma instabilities. There are many astrophysical objects, both relativistic and non-relativistic, that

show these characteristics such as in Supernova remnants and gamma-ray bursts [Ref]. When a supernova event occurs, the plasma ejecta stream from the explosion and go through interstellar media, encountering various physical conditions. Among those, Weibel instabilities are created from their momentum anisotropy distribution [4]. Conceptually, the Weibel instabilities create self-generated magnetic fields; then the plasma ions are trapped within the magnetic fields via the Lorenz force; the ion trajectory in the interpenetrating plasmas is sufficiently trapped creating localized heating, i.e. a collisionless shock is formed (Fig. 1). The most significant aspect of these instabilities is their conversion from kinetic energy to magnetic energy that can be the mechanism for seed magnetic fields in universe [5]. The signature of the instability is a pattern of current filaments stretched along the axis of symmetry of the electron distribution. The exact understanding of the required physical condition for such occurrence has not been well characterized. Laboratory laser experiments can provide a unique platform to study the electromagnetic Weibel instabilities that occurs from high-Mach number plasma flows. There are many scenarios in astrophysics where self-organization involving magnetic or electric fields in collisionless settings is observed. Examples include the generation of the cosmic magnetic field, collisionless shocks in supernova remnants, relativistic shocks and particle acceleration in gamma-ray bursts, and internal structures in star forming regions of molecular clouds.

2. Experimental set-up

Figure 2 shows our typical laser experimental configuration at the Omega laser facility [ref]. Two face-on polystyrene (CH_2) plastic foils are illuminated by ~4 kJ of 351 nm laser energy with focal spot diameter of 250 μm on the target surface, generating high-velocity counter-streaming plasma flows. The separation is 8 mm between the targets. We employ Thomson scattering diagnostics to understand the plasma bulk velocity (v), electron temperature (T_e), ion temperature (T_i) and electron density (n_e), The Thomson-scattered (TS) light from the 526.5 nm probe studies the plasma volume of 100 μm x 100 μm x 60 μm at the central region of the counter-streaming plasmas. Thomson scattering is measured from the electron feature (collective scattering from electron-plasma waves) and the ion feature (collective scattering from ion-acoustic waves) [6]. An example of time composite electron and ion features from the double foil counter-streaming data is shown in the top right panel in Figure 2.

Another key element of our experiment is proton probing to understand the magnetic field structures. We use 2 different proton sources: 1) by short pulse generated protons; 2) by imploding a capsule filled with deuterium (D) and ^{3}helium (^{3}He) fuel. The short pulse generated protons are generated by illuminating a 10 ps pulse of up to 800 J of 1053 nm infrared light onto 40 μm diameter spot for an intensity of ~$2x10^{18}$ W/cm^2 on an Au disk target. Electric and magnetic fields deflect the protons which are then recorded on a radiochromic film layered with Al filters to obtain a range of proton energies from 5 to 15 MeV. We also use the 14.7 MeV mono-energetic proton source generated by thermonuclear interaction of D+^{3}He $\rightarrow$ ^{4}He+p [7]. For our experiments, the 2 μm thin silica capsules are filled with 18 atm D^{3}He fuel (6 atm of D and 12 atm of ^{3}He for equal atomic distribution) and are compressed uniformly by ~9 kJ of laser energy from 18 laser beams. The protons are generated at the peak of compression creating ~10^8 protons isotropically lasting ~50 ps with a source size of ~50 μm in diameter. These protons are detected using CR39 film in which the proton tracks are etched and counted to form an image. Examples of proton magnetic field imaging are shown in the right-bottom panel in Figure 2.

3. Thomson scattering results

Extensive Thomson scattering data were is collected for both single-flow and counter-stream flows. Time-slices of the data from the electron feature are then fitted with the Thomson scattering form factor allowing a measurement of the electron temperature (T_e) and electron density (n_e). With constraints from the electron feature fitting, the ion feature can then be used to measure the ion

temperature (T_i) and bulk plasma flow velocity (v). This can be understood from the simplified dispersion relation, $\Delta \lambda = \frac{4\lambda_{p\_r}o^{\:ih_{D}\omega}}{c} s^{\:i\mathcal{O}n\mathcal{Q}} \sqrt{\frac{ZT_e}{M} + \frac{3T_i}{M}}$. Figure 3 shows the summary of the resulting plasma parameters of v, n_e, T_e and T_i, where single flow is noted in red and the counter-streaming double flows are marked in blue respectively.

The bulk flow velocity (Fig 3 (a)) is $> 10^8$ cm/s (>1000 km/s) up to 5 ns and is not supressed even for the double flow case. The single flow n_e is ~5×10^{18} cm^{-3} at maximum and is doubled for the counter-streaming case at 1×10^{19} cm^{-3}. This indicates that a shock is not quite fully formed as we should expect a factor of > 2 increase in electron and ion densities when a shock is formed. A more surprising discovery is the 2x more increase in Te and Ti. The Te was ~100 eV for the single flow whereas the double flow Te was up to 1 keV, a factor of 5 increase. The rapid Te increase at early time is explained by electron-ion collisions from ion slowing-down by drag forces caused by the 'resting' electron gas [8]. The relative velocity of the electron gas and each of the ion streams leads to the appearance of the electron-ion drag force. Analytic calculation of the electron temperature increase from this model is plotted in black solid line in Fig 3 (c) showing that the model agrees well with the data at early time. Ignoring the electron thermal conduction in this model explains the late-time discrepancy. While this drag-force model explained the Te increase very well, the ion-ion collisions could not explain the observed Ti increase. When collision Particle-in-Cell simulations are applied accounting for acoustic two-stream electrostatic instabilities, we are able to reproduce the Ti increase. [one more sentence] Our quantitative plasma state measurements suggest that the intra-flow ion and electron collisional effects are important and that inter-flow ion collisions are rare from high velocity flows.

4. Observation of self-organizing fields

Using proton probe short pulse lasers on EP, we observe large, stable, reproducible electromagnetic field structures that arise in counter-streaming interpenetrating supersonic plasma flows in the laboratory. Self-organization, whereby energy progressively transfers from smaller to larger scales in an inverse cascade, is widely observed in fluid flows, such as in the nonlinear evolution of multimode Rayleigh-Taylor and Kelvin-Helmholtz instabilities. These surprising structures, predominantly oriented transverse to the primary flow direction, extend for much larger distances than the intrinsic plasma spatial scales, and persist for much longer than the plasma kinetic timescales [9]. One such example image is shown in Fig 4 (a). This image is taken at 5.2 ns after the laser, and the sharp co-planar field structures are clearly visible. Their origin is now explained by the magnetic field advection process. Here the Biermann battery magnetic field is generated near the target surface in a toroidal shape, and advects along the electron plasma flows, then recompresses near the midplane [10]. A sketch of this process is shown in Fig 4 (b) and (c). The magnetic field strength is evaluated by the caustic analysis [9] by: $B_{cf} = \frac{m_p c}{el} \sqrt{\frac{2W}{m_p}} \frac{d^3}{\sqrt{\pi} a^2 b \sin \psi}$, where W is the proton kinetic energy (8.8 MeV), b/a the aspect ratio (1/20), l is the distance from proton source to object plane (8 mm), ψ is the tilt angle of the plane (5 to 10 degrees). When we apply our experimental measurements and observables, we derive $B_0 = 10T$. The observed plasma self-organizing magnetic field may play an important role in astrophysics how electromagnetic order emerges from high-velocity plasma flows.

5. Observation of Weibel filamentation

We recently used a D^{3}He imploding capsule to create a mono-energetic proton source and imaged the counter-stream double flows. The result was quite spectacular as shown in Fig 5 (a) where filamentary striation field features are clearly visible along with the co-planar structures. We study whether these filaments could be generated by Weibel instabilities (filamentation is the characteristic morphology for Weibel instabilities.) There have been many Particle-in-Cell simulations that show magnetic field

filamentary structures. However, the field spatial scales, magnetic field strength, and their density can be misleading when a proton probe is used. In order to understand both the Weibel and Biermann battery generated magnetic fields in our proton imaging experimental system, we have conducted detailed 3-dimensional particle-in-cell (3D PIC) simulations along with proton ray tracing through the electromagnetic field (a schematic is shown on the left panel in Fig 5.) In addition to the filamentary structure, we also added the Biermann battery field that was described in section 4. The plasma input is also from our experimental measurements as described in section 3: n_e=5x10^{18} cm^{-3}, v_e=v_i=1000 km/s, T_e=T_i=100 eV. The simulation results are shown in Fig 5 (b) showing remarkable resemblance to the data. From the detailed studies of simulation and data, we derive the magnetization, which is defined: $\sigma = \dfrac{B^2/4\pi}{(\gamma-1)nmc^2}$. This is the quantity that the kinetic energy converts to magnetic energy in the system. Figure 6 shows this magnetization as a function of time. The dotted line is the field strength without pre-existing magnetic field where as the solid line is accounting for the initial field by the Biermann battery. The straight linear line is the theoretical growth rate of the ion Weibel instability. Note that the final total magnetization is 0.01 and the initial Biermann battery field plays little role in the magnetization growth. This result is the first time the Weibel instability filamentation is clearly observed in the laboratory and measures a significant self-generated magnetization [Ref].

6. NIF experiments

While the Omega experiments produced a remarkable understanding of counter-streaming plasmas, we note that the Weibel mediated collisionless shock is not fully formed as indicated by the electron density measurements and the field formation in the 3D PIC simulation results. Our NIF experimental configuration will apply ~100 kJ per target and separation of 8 mm. The radiation hydro simulation (HYDRA) of our single flow simulation is shown in Fig 7 indicating we will have much higher ne (>1020 cm-3), Te (>1 keV) and higher flow velocity (>2000 km/s). This will produce a well-formed shock as the ion skin depth will be much shorter and a high magnetic Reynolds number will favor producing higher magnetization. Using this flow condition, the 3D PIC simulation (Fig 8) predicts a much higher magnetic field generation of up to ~3 MG (top row) and a shock density of n/n$_0$ ~4. On NIF we will use the D3He generated proton source to image the magnetic field structures and x-ray and neutron spectroscopy to measure the plasma state.

In conclusion, the laser generated counter-streaming plasma flows are studied in connection to the astrophysical collisionless shocks. We observe that the intra-collisional electron-ion interaction by electron-drag force elevates the electron temperature and electrostatic instabilities upraise the ion temperatures for the double flows. We detect very stable self-organizing field structures that originat from the recompression of the advected Biermann battery magnetic field. The Weibel filamentation is directly imaged first time and the magnetization level at 0.01 is derived. The NIF experiment will be able to create true Weibel mediated collisionless shocks.

References
[1]   Ross J S et al. 2013 *Phys. Rev. Let.* vol 110 p 145005
[2]   Kugland N et al. 2012 *Nature Physics* vol 8 p 809
[3]   Huntington C M et al. 2013 *Nature Physics*, submitted
[4]   Weibel E S 1959 *Phys. Rev. Let.* Vol 2 p 83
[5]   Medvedev M V et al. 1999 *Astrophys. J* vol 526 p 697
[6]   Ross J S et al. 2010 *Rev. Sci. Inst.* 81, 10D523.

[7]   Li C K et al. *Rev. Sci. Inst.* 2006 77 10E725
[8]   Ross J S et al. 2012 Phys. Plasmas 19 056501
[9]   Kugland N L et al. 2013 Phys. Plasmas. 20 056313
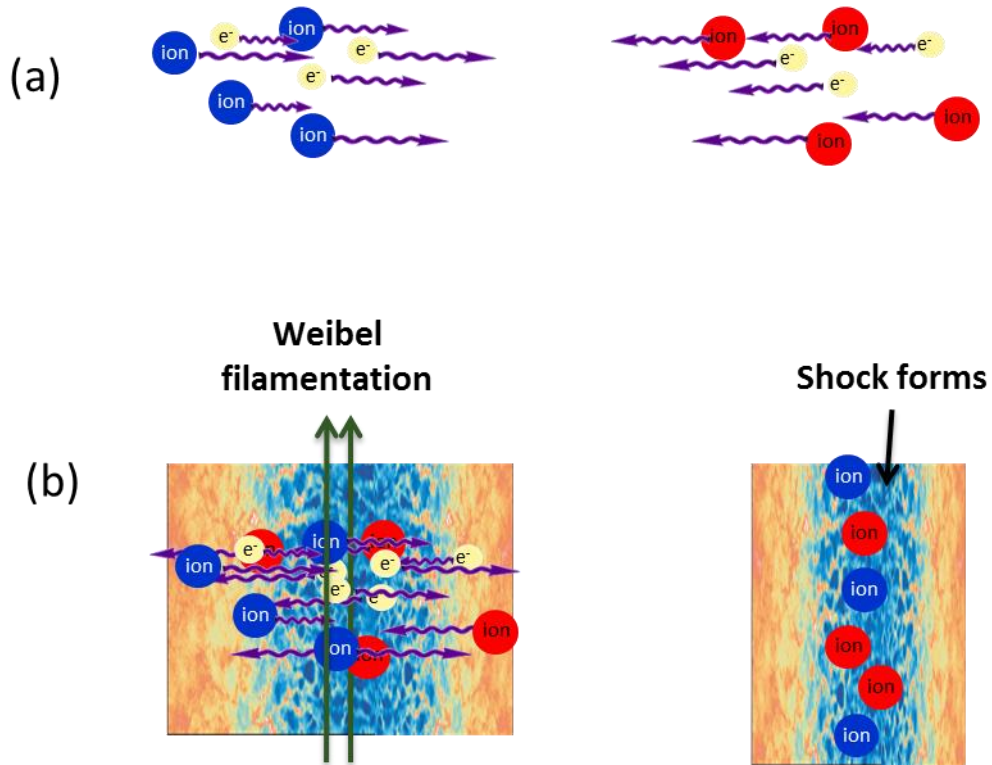[10]   Ryutov D D et al. 2013 Phys. Plasmas. 20 032703

Figure 1. (a) interpenetrating counter-streaming plasmas where Coulomb mean-free-path is much larger than the system size; (b) Weibel instabilities traps the ions via self-generated magnetic fields and creates the collionless shocks.
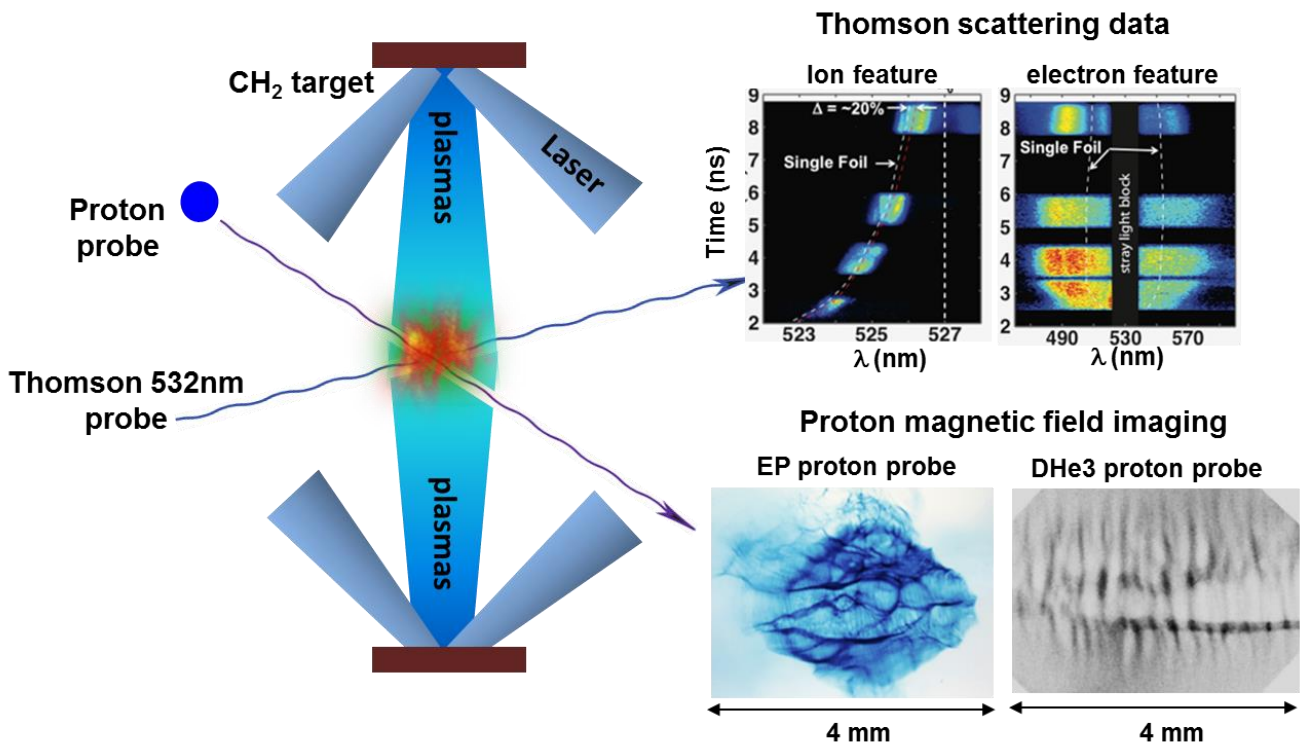
Figure 2, Schematic of Omega experiment. We use Thomson scattering to probe the plasema state and proton probe to image the magnetic field structures.
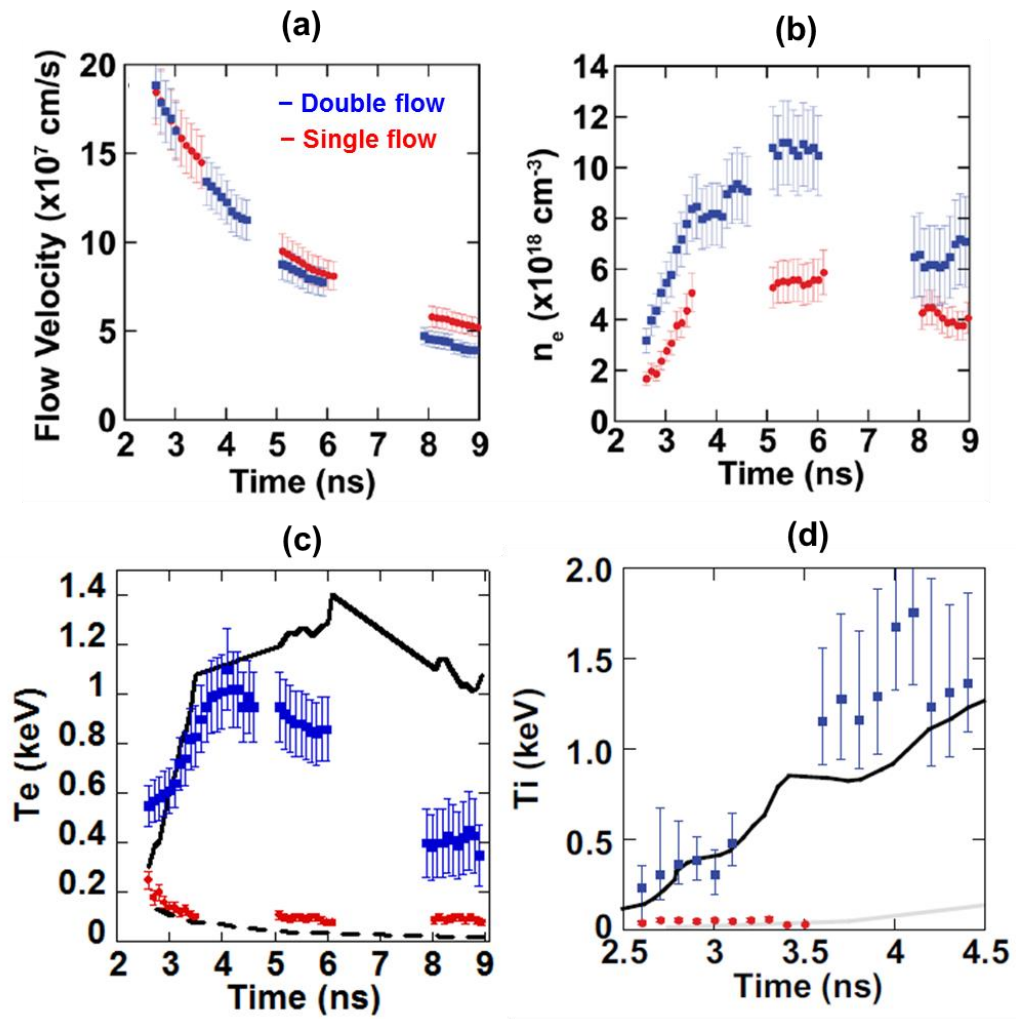
Figure 3. Omega Thomson scattering results for both single and double flows. The high increase in Te and Ti are due to electron drag force and the electrostatic instabilities
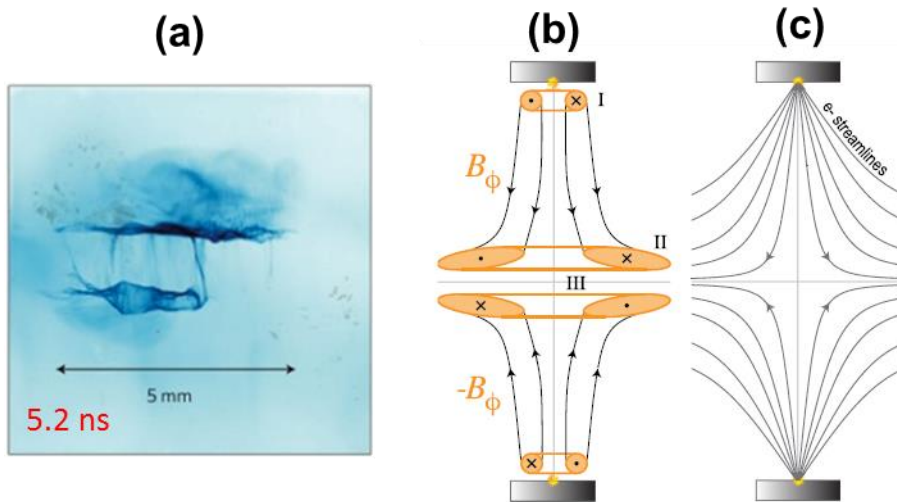
Figure 4. Omega EP short pulse generated proton image of counter-streaming plasmas at 5.2 ns after the laser. Highly stable self-organizing planar magnetic field structures are observed (Fig. a). This is from the Biermann battery magnetic field that is generated near the target surface; advects along the electron flows; then recompress in the mid-plane.
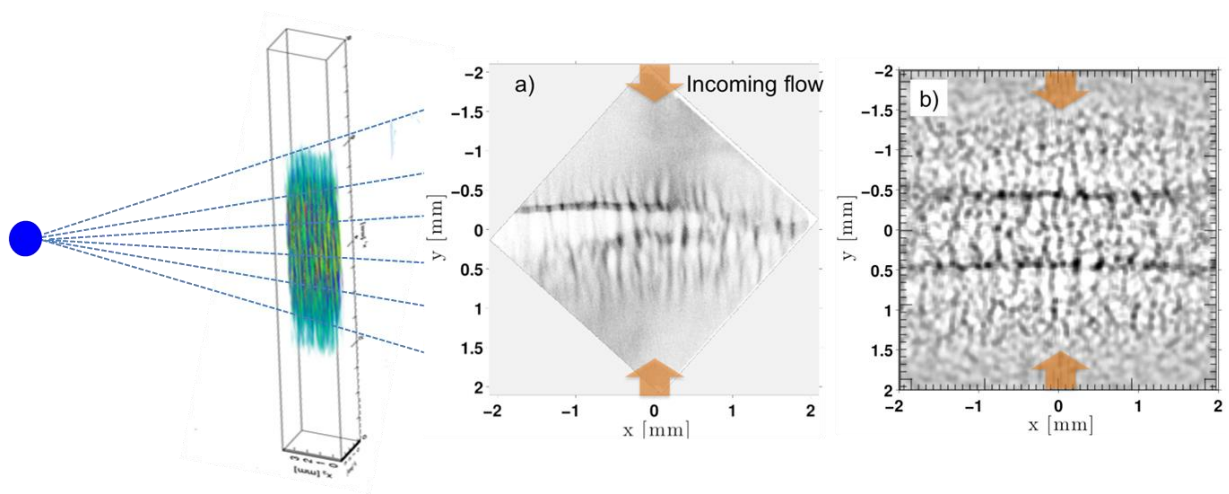
Figure 5. Schematic of proton image of D3He3 imploding capsule. (a) is the experimental data where the Weibel filamentary structures are clearly observed; (b) is the 3D Particle-in-cell simulation and the proton ray trajectory from experimental angle. The simulation also added Biermann battery field that shows as the band structure in the middle.
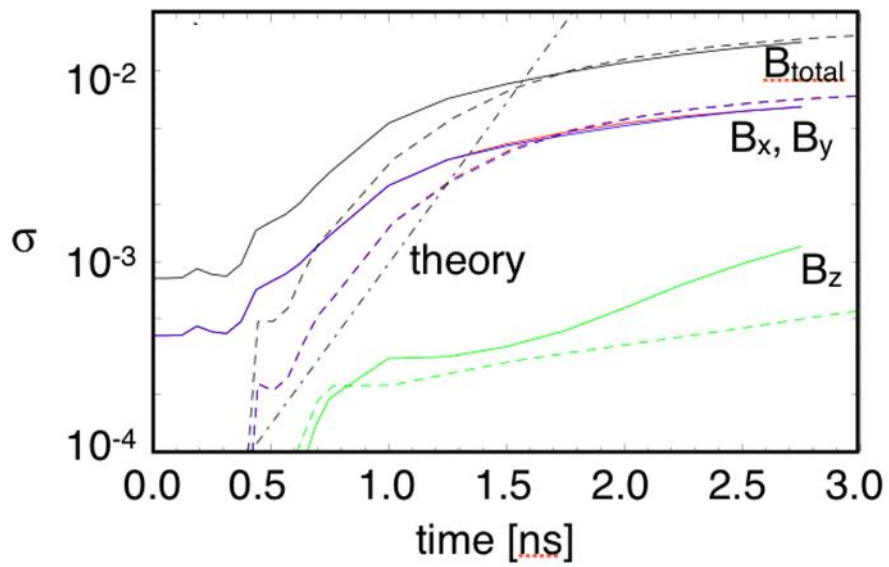
Figure 6. Magnetization level derived from the PIC simulation after matching the condition of the Omega data results as shown in Figure 5. The dotted lines are with zero initial magnetic field condition whereas the solid lines are with the initial condition of Biermann battery field that matched the data. Note that the Biermann battery field plays little role in the final B-field strength. The straight line is the theoretical Weibel mediated B-field growth. The magnetization is achieved up to 1% level.
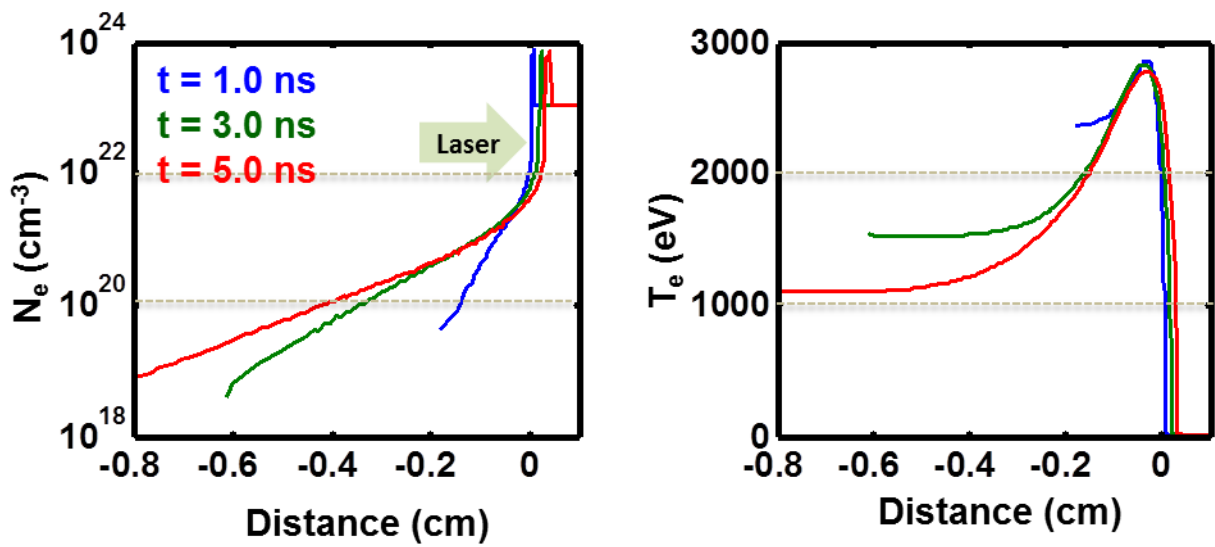
Figure 7. HYDRA simulation results for the NIF experimental condition with 100 kJ per target condition. The different color represents the pulse duration. At 5 ns setting, the N_e is $\sim 10^{20}$ cm^{-3} and the T_e is ~ 1 keV at 4 mm from the target surface.
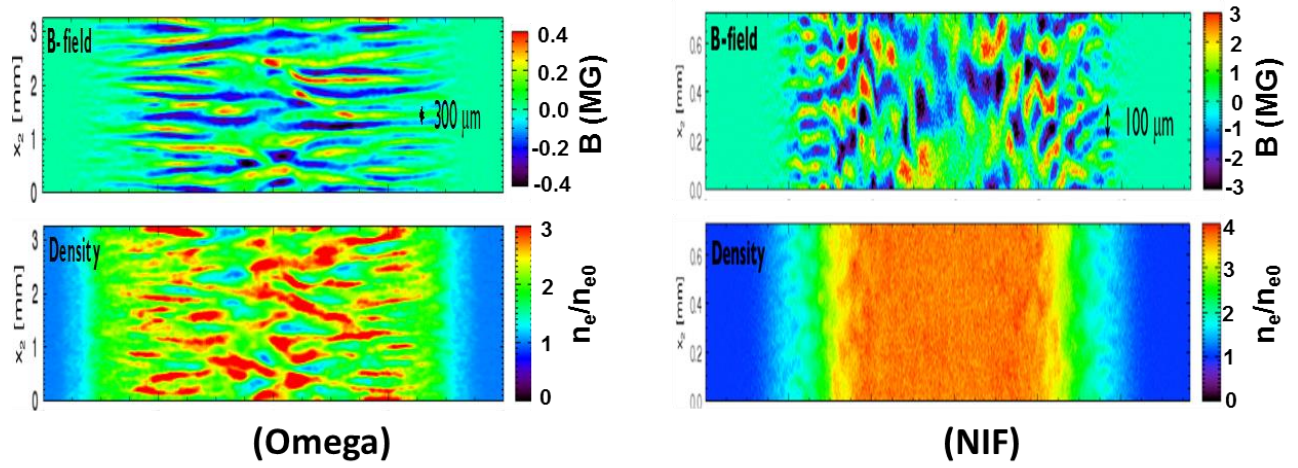
Figure 8. 3D PIC simulation results of B-field (top row) and electron density (bottom row) for Omega and NIF cases. The NIF experiments will be able to produce fully formed collisionless shocks (n_e/n_e0 ~4) and B field near 3 MG.